Correlations between heavy mesons and the creation of the charmonia, bottomonia, and B_c mesons in high energy pp collisions

Jiaxing Zhao,[1,2,3] Joerg Aichelin,[1] Pol Bernard Gossiaux,[1] and Klaus Werner[1]

[1]*SUBATECH, Nantes University, IMT Atlantique, IN2P3/CNRS, 4 rue Alfred Kastler, 44307 Nantes cedex 3, France*

[2]*Helmholtz Research Academy Hessen for FAIR (HFHF), GSI Helmholtz Center for Heavy Ion Research, Campus Frankfurt, 60438 Frankfurt, Germany*

[3]*Institute for Theoretical Physics, Johann Wolfgang Goethe Universität, Frankfurt am Main, Germany*

(Received 22 November 2025; accepted 30 April 2026; published 16 June 2026)

The different QCD processes, which can produce a heavy quark-antiquark ($Q\bar{Q}$) pair, induce different correlations between the heavy quarks. Employing the EPOS4HQ event generator, we study the consequences of these correlations and compare the calculation with experimental results on open and hidden heavy flavor mesons, measured in proton-proton (pp) collisions at RHIC and LHC energies. We find that the measured correlations between heavy mesons are a direct image of the different ways in which the heavy quark pair is produced. They also contribute differently to the transverse momentum distribution of open and hidden heavy flavor mesons. The latter are calculated in a Wigner density approach, which also enables us to reproduce quantitatively the measured B_c spectra. This agreement allows conclusions on the spatial distribution of the heavy quark creation processes.

DOI: 10.1103/6c95-5r3p

I. INTRODUCTION

In the last decade, heavy flavor (HF) hadrons have turned out to be one of the most promising probes to study the properties of the expanding quark gluon plasma (QGP) produced in ultrarelativistic hadronic collisions. Open heavy flavor hadrons have been the object of investigation of quite a number of transport approaches [1–14], which succeeded to describe the experimentally observed multiplicity of the different mesons and baryons, as well as three key observables—the transverse momentum, p_T; dependence of the elliptic flow, v_2—and the ratio between the yield measured in heavy ion collisions and in proton-proton (pp) collisions, scaled by the number of initial hard scatterings, R_{AA} [15–20]. These transport approaches have even revealed that the enhanced multiplicity of charmed baryons, as well as the unexpected elliptic flow of charmed mesons, can be well understood if one assumes also that in systems as small as pp, a QGP is created.

Correlations between open heavy flavor hadrons as well as hidden heavy flavor mesons have been much less in the focus of theoretical studies, although several experimental observations have come as a surprise and pose challenges to transport approaches. The heavy quark azimuthal correlation function, measured by LHCb in forward rapidity [21], shows a very pronounced structure. The observed values of R_{AA} of J/ψ at low p_T is very different at RHIC [22] as compared to LHC energies [23], and the observed v_2 of J/ψ is finite at LHC [24], whereas that observed at RHIC is compatible with zero [25]. For LHC energies, this points toward an interaction of the quarkonium (or of the heavy quarks, which form it later) with the expanding QGP, because initially single charm quarks are isotropically distributed in the azimuthal direction. In this work, we will demonstrate that correlations between open heavy flavor mesons and the production of quarkonia are two sides of the same coin, because both are sensitive to the azimuthal angle between the Q and $\bar{Q}$ at production. The production of heavy quark ($Q\bar{Q}$) pairs can be described by perturbative QCD, due to $m_Q \gg \Lambda_{\mathrm{QCD}}$, with a heavy quark mass m_Q and the QCD cutoff Λ_{QCD}, and the single-particle distribution has been calculated in FONLL [26,27] based on QCD perturbation theory. The results agree quite well with the experimentally observed single-particle p_T distribution.

Azimuthal correlations between $Q\bar{Q}$ pairs have been studied in a couple of event generators [28–31]. The comparison with experimental data shows that there is considerable improvement necessary if one would like to obtain them from the measured correlation information about the underlying production processes.

Also, the formation of colorless quarkonium states from a given heavy quark pair $Q\bar{Q}$ contains information on the azimuthal correlations between the heavy quarks. It is a nonperturbative process and has been studied via many approaches, such as the color-evaporation model (CEM) [32–34], the color-singlet model (CSM) [35,36], and the color-octet model (COM) [37], the latter two being encompassed in effective theories [38–41].

Recently, we have advanced a new approach, which is based on the quantum density matrix and which has turned out to give a very good description of the quarkonium p_T spectra in pp—not only for the J/ψ, but also for the excited states [42–44]. For this study, the underlying momentum distribution of the $Q\bar{Q}$ is given by the EPOS4 event generator, in which different processes contribute to the production of a $Q\bar{Q}$ pair. The purpose of this paper is, on the one side, to extend this analysis to hidden bottom mesons and to the formation of B_c, and on the other side, to show how the initial correlations between the heavy quarks show up in correlations between two open heavy flavor hadrons and in hidden heavy flavor observables in order to establish how these correlations can be assessed experimentally.

For our study,[1] we use the EPOS4 event generator [45–48], which has been shown to reproduce a multitude of light flavor observables. In its extension to heavy quarks, EPOS4HQ, it nicely reproduces as well the available open heavy flavor data in pp [49], as well as in heavy ion collisions [14] at RHIC and LHC energies.

The paper is organized as follows: In Sec. II, the elementary $Q\bar{Q}$ production in EPOS4 is analyzed, while the model for quarkonium production and its predictions are provided in Sec. III. Section IV contains our conclusions.

II. $Q\bar{Q}$ PRODUCTION IN EPOS4HQ

A. Mechanisms to produce $Q\bar{Q}$ pairs

In EPOS4HQ, pp interactions are described by the exchange of Pomerons [47]. The unique feature of EPOS4 is a systematic treatment of multiple scattering, in the framework of S-matrix theory. A recent series of four basic publications [45–48] explains this approach in great detail—in particular, the relation between a environment-dependent saturation scale and the fact that the multiple-scattering approach agrees with factorization in the case of inclusive scattering. Therefore, EPOS4 does not use parton distribution functions as input, as practically all other models do. EPOS is therefore also not a fixed-order calculation. This feature it shares with with other event generators like PYTHIA [50] and POWHEG + HERWIG [51], which are also not fixed-order calculations once the hard process is connected to the parton shower.

EPOS4 combines the hard processes with the parton shower and neglects interference terms as they appear between the soft gluon emission of a heavy (anti)quark after the LO process and the NLO gluon splitting. We do not expect that this influences the result at small ($\Delta\phi \approx 0$) or large ($\Delta\phi \approx \pi$) azimuthal opening angles between the heavy quark pairs, because kinematically, flavor creation and gluon splitting have little overlap. For a discussion of the production of heavy quark pairs in NLO calculations, we refer the reader to Ref. [52].

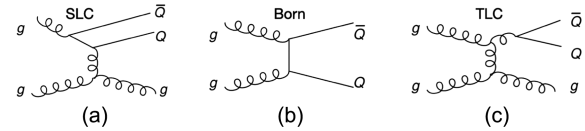

FIG. 1. The three ways in which heavy quark pairs are produced. From left to right: flavor excitation, flavor creation, and gluon splitting. For details, we refer to the text.

In EPOS4, $Q\bar{Q}$ pairs can be created in three leading-order or next-to-leading-order processes, which are displayed in Fig. 1. They can be created from a timelike gluon, which disintegrates into a $Q\bar{Q}$ pair after the gluon has been produced in the hard collision between the partons from the projectile and target. This process is called "gluon splitting" and is shown in the rightmost diagram. It can be produced by gluons as well, which are emitted during the spacelike cascade (SLC) of the partons before the hard scattering process. In the hard process between the projectile and the target partons, mediated by a gluon exchange, the $Q\bar{Q}$ pair then gets on the mass shell. This process, shown in the left diagram of Fig. 1, is called "flavor excitation." A $Q\bar{Q}$ pair can also be produced in the hard collision between the projectile and target partons, displayed in the middle diagram. This leading-order process is called "flavor creation." In addition to these basic processes, higher-order terms contribute as well, due to the realization of full spacelike and timelike cascades (TLC); see Ref. [46].

In this paper, we employ EPOS4HQ, which was introduced in Refs. [14,49]. In distinction to EPOS4, in EPOS4HQ heavy quarks can interact with the QGP, which is formed if the critical energy density of particles produced in hard collisions is higher than 0.57 $\mathrm{GeV/fm^3}$ [48]. The formation of a QGP has a significant influence on some observables, like on the elliptic flow and on the chemistry of charmed baryons, but it leaves other HF observables, such as momentum spectra and correlations, practically unchanged; see Ref. [49].

B. $Q\bar{Q}$ azimuthal correlations

Already from the kinematics, one can expect that the different processes yield quite different correlations between the Q and the $\bar{Q}$. For flavor creation, one expects in the center of mass of the heavy quark pair a back-to-back emission, whereas for gluon splitting the kinematics is determined by the gluon, and one expects a small angle between the Q and $\bar{Q}$. The importance of the different processes depends strongly on the energy and on the kinematic region where the correlations are studied. It is also different for bottom and charm quarks.

[1]Based on version EPOS4.0.4.q4.

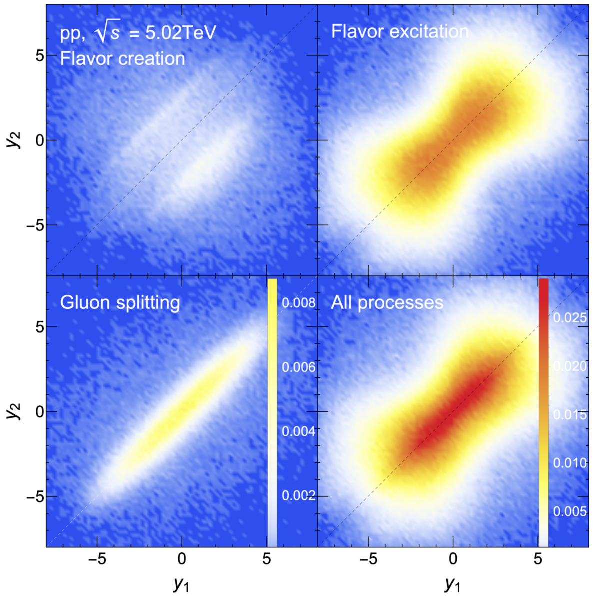

FIG. 2. The correlation between the rapidities of c and $\bar{c}$ from different processes in pp collisions at $\sqrt{s} = 5.02$ TeV.

The correlations between the c and $\bar{c}$ quark at creation, produced in pp collisions with $\sqrt{s} = 5.02$ TeV, are shown in Figs. 2 and 3 in a density plot for the different creation processes. In Fig. 2, we display the correlation between the rapidities; in Fig. 3, we show that between the transverse momenta of the charm quark and the antiquark. We see, first of all, that there exist strong correlations between the c and $\bar{c}$ created at the same vertex. In the flavor creation process, the heavy quarks are centered around two bands. The maximum of these bands is at $y_1 = -y_2 = \pm 1.5$. We expect that $y_1 = -y_2$ from back-to-back emission in the pp center-of-mass system. Because initially the quark-antiquark pair or gluon pair, which enters the hard process and which creates the $c\bar{c}$ pair, has negligible transverse momentum, in the flavor creation process the heavy quarks have an opposite transverse momentum. We observe indeed a very strong correlation in transverse momentum space between the two heavy quarks. The rapidity distribution of heavy quarks produced by flavor excitation peaks at midrapidity. The correlation between the heavy quarks is, however, not very strong, since one of the heavy quarks gets a kick in the hard process (Fig. 1, left). In this kick, transverse momentum is also transferred to the heavy quark. Therefore, one of the heavy quarks has a considerably larger transverse momentum than the other, as seen in the transverse momentum correlation. In the gluon-

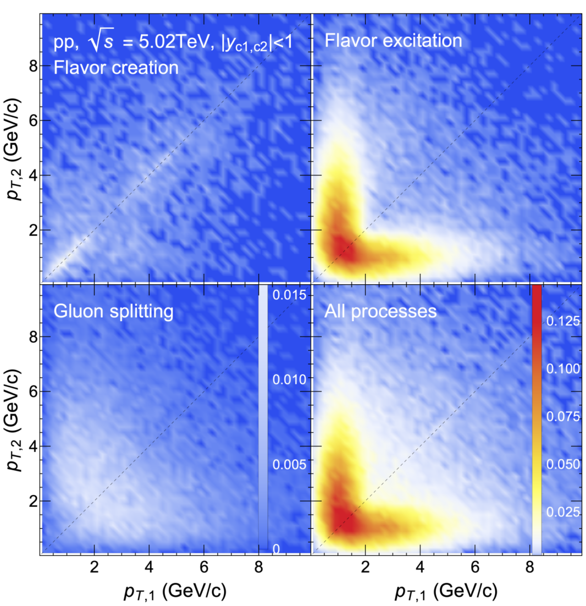

FIG. 3. The correlation between the p_T of c and $\bar{c}$ from different processes in pp collisions at $\sqrt{s} = 5.02$ TeV and central rapidity $|y| < 1$.

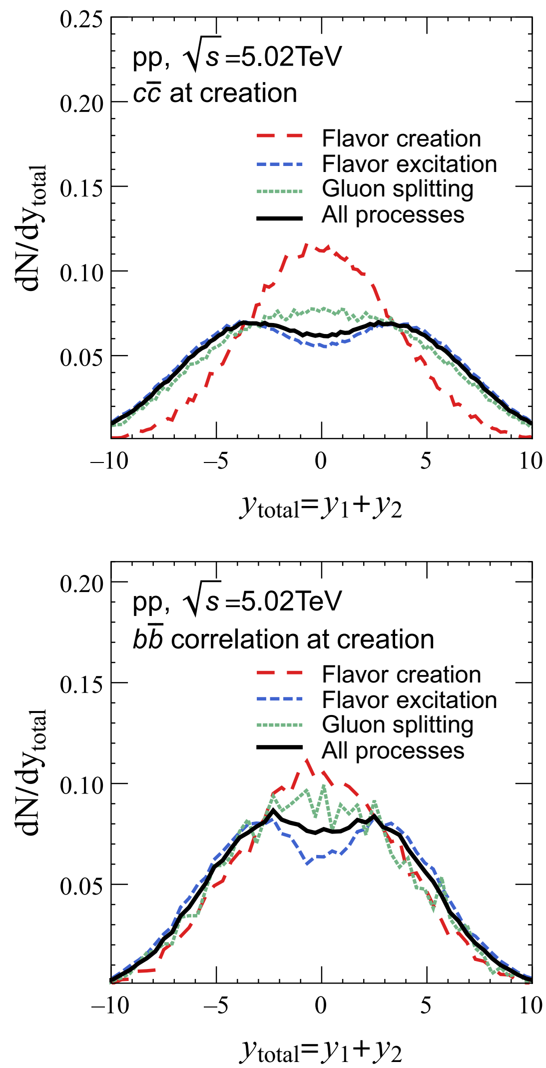

FIG. 4. The normalized distribution of the total rapidity of c and $\bar{c}$ (upper), and that of b and $\bar{b}$ (lower) for different processes in pp collisions at $\sqrt{s} = 5.02$ TeV.

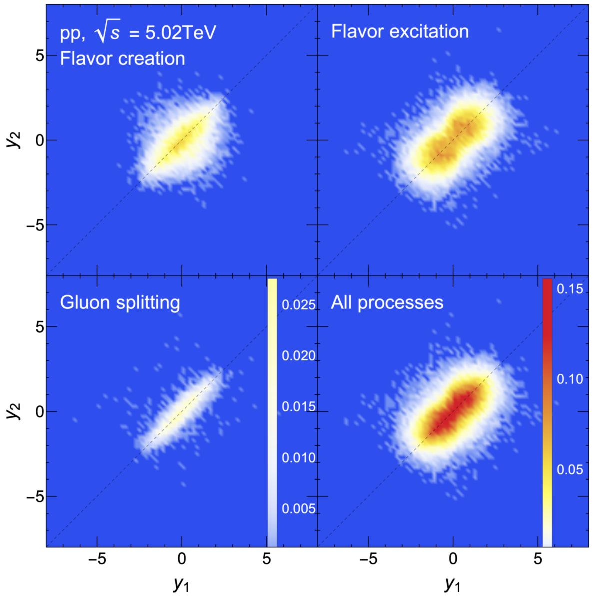

FIG. 5. Same as Fig. 2, for $b\bar{b}$ pairs.

splitting process, the rapidities are strongly aligned, reflecting the rapidity of the gluon, which disintegrates into the pair (Fig. 1, right). The transverse momenta are correlated very little, as a recoiling parton opposed to the gluon carries away a significant transverse momentum. As we will discuss later, flavor excitation is the dominant process for $c\bar{c}$ production at low p_T, and therefore, if we add up all processes in the bottom-right figures, we will see that the correlation pattern is governed by the flavor excitation processes.

The normalized distribution of the sum of the rapidities of the $c\bar{c}$ pair is displayed in Fig. 4. The distribution due to flavor creation and gluon splitting is centered around midrapidity. In the flavor excitation process, the rapidity distribution of heavy quarks shows a maximum at a finite y_{total}, because one of the quarks receives a finite-momentum kick in the hard interaction.

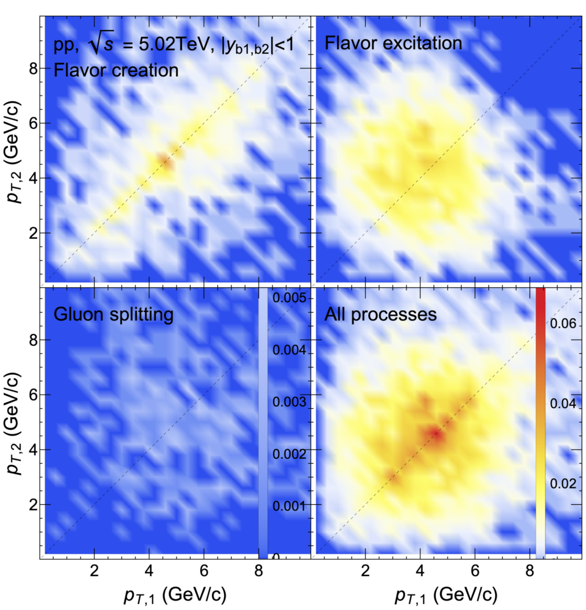

FIG. 6. Same as Fig. 3, for $b\bar{b}$ pairs.

Figures 5 and 6 show the y and p_T correlations for $b\bar{b}$ pairs. For b quarks, the flavor creation process yields quarks, which are centered at equal rapidity, because only in this kinematics is sufficient energy for the production of b quarks available. In the flavor excitation process, the kick of one of the quarks due to the hard process is accompanied also by a rapidity transfer. Gluon splitting is much less important for b quarks, because the gluon energy for this processes is less frequently available. Also, for b quarks created by flavor creation, the transverse momenta of the two quarks have the same magnitude. The average p_T of the b quarks created by flavor excitation, is larger than that for the c quarks and centered around $p_{T1} \approx p_{T2}$.

The p_T integrated azimuthal correlations between the $Q\bar{Q}$ pair for finally observed mesons for $p_{TQ}, p_{T\bar{Q}} >$ 2 GeV are displayed in Fig. 7 for charmed quarks (mesons) and in Fig. 8 for bottom quarks (mesons). We display in the top row the correlations of the heavy quarks at production, and in the bottom row those for the finally observed open heavy flavor mesons. In the left row, we see the results for mesons observed with $|y| < 1$, and the right row displays those for forward-emitted mesons $2 < y < 4$. We separate the correlations for the different ways in which heavy quark pairs are produced. The dashed red line shows the results for quarks produced in a flavor creation process, the short-dashed blue line those produced in a flavor excitation

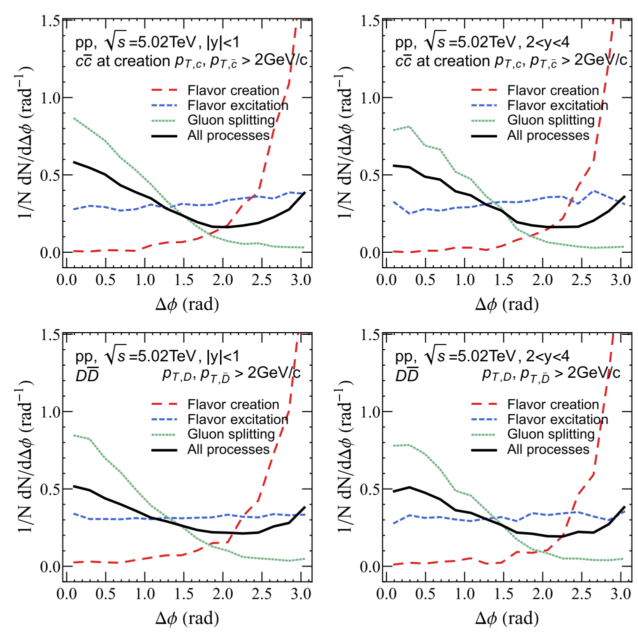

FIG. 7. Correlation of $c\bar{c}$ quarks with $p_T > 2$ GeV from the same vertex at creation, and that of $D^0\bar{D}^0$ mesons with $p_T >$ 2 GeV in pp collisions at $\sqrt{s} = 5.02$ TeV, with central rapidity (left) and forward rapidity (right).

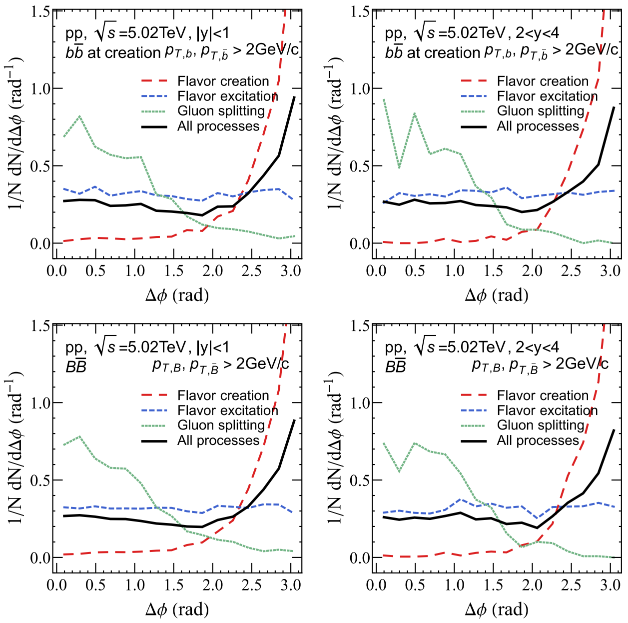

FIG. 8. Correlation of $b\bar{b}$ with $p_T > 2$ GeV from the same vertex at creation, before hadronization, and that of $B\bar{B}$ with $p_T > 2$ GeV in pp collisions at $\sqrt{s} = 5.02$ TeV, with central rapidity (left) and forward rapidity (right).

process, and the dotted green line those from gluon splitting. The thick black line is the sum over all processes, as seen in experiment. We observe for all gluon creation processes quite different correlations; however, they do not change much with centrality. As expected, the transverse momenta of $Q\bar{Q}$ pairs created by flavor creation are back-to-back, and therefore the azimuthal opening angle peaks at π. On the contrary, those produced by gluon splitting have a small opening angle, whereas those produced by flavor excitation show an almost flat distribution as a function of the azimuthal opening angle.

If one sums over all processes, the azimuthal correlations between $c\bar{c}$ pairs still show a enhancement for $\Delta\phi = 0$ and $\Delta\phi = \pi$. Since gluon splitting is more important than flavor creation, the enhancement at $\Delta\phi = 0$ is larger. It is remarkable that the correlation function remains almost unchanged from the initial heavy quark production to the finally observed heavy meson in pp collisions. Hence, heavy flavor correlation experiments offer the opportunity to study the importance of the different leading-order and next-to-leading-order heavy flavor creation processes and their kinematics.

For the $b\bar{b}$ pairs, the dominance of the back-to-back emission remains visible, even after summing over all processes. For low $\Delta\phi$, the spectrum is almost flat due to production by gluon splitting having little importance. Also, for bottom quarks, the initial correlation is almost identical to that of the final B mesons.

The difference between the correlation functions of D and B mesons has also been observed experimentally. In Fig. 9, we compare our calculations with the available

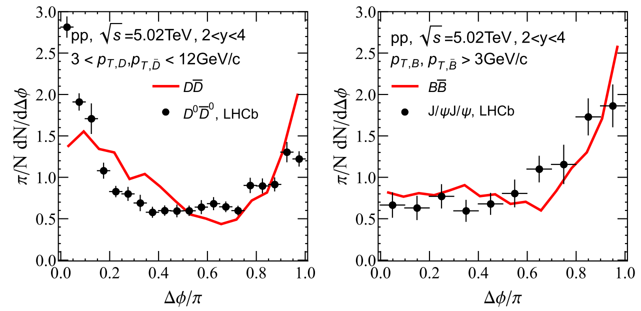

FIG. 9. Experimental correlations in comparison with EPOS4 results. *Left:* $D^0\bar{D}^0$ correlations in pp collisions at $\sqrt{s} = 7$ TeV in comparison with LHCb data [21]. *Right:* EPOS4HQ $B\bar{B}$ correlations in comparison with the experimental correlations of nonprompt J/ψ from B decays in pp collisions with $\sqrt{s} = 7$ TeV [53].

experimental results of LHCb. On the left-hand side, we compare the measured $D^0\bar{D}^0$ azimuthal correlations for $2 < y < 4$ and $3 < p_T < 12$ GeV with the $D\bar{D}$ results of EPOS4HQ. First of all, we see that due to the higher p_T cut ($p_T > 3$ GeV), the $D\bar{D}$ correlations due to the three different ways in which heavy quark pairs are produced become even more visible. The $B\bar{B}$ correlations, shown on the right-hand side, are different. We have to add here a warning: The b hadrons disintegrate into a J/ψ via many different channels, and for none of them is the explicit kinematics known. Therefore, we compare here the measured $J/\psi J/\psi$ correlation with the calculated $B\bar{B}$ correlation, neglecting the fact that the disintegration of the B into

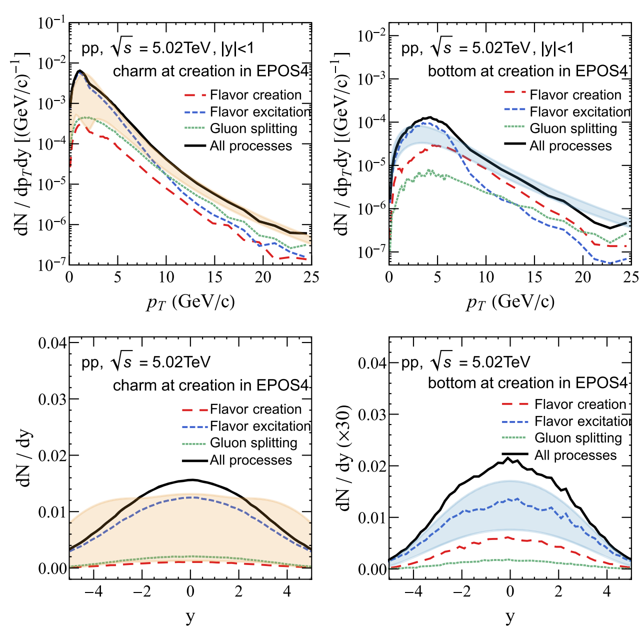

FIG. 10. p_T spectrum and rapidity distribution of charm (left) and bottom quarks (right) in pp collisions at $\sqrt{s} = 5.02$ TeV. The band is the FONLL calculation [26].

a J/ψ smears out the correlation. We see clearly the enhancement due to back-to-back emission in the flavor creation process, but as discussed, the enhancement of creation with a small azimuthal opening angle is much less visible than for $D\bar{D}$ creation. This is a consequence of the different relative contributions of the different heavy quark creation processes. Both the $D\bar{D}$ and the $B\bar{B}$ azimuthal correlations are well reproduced in EPOS4HQ.

C. Single-particle spectra

It is interesting to see how the different ways in which heavy quark pairs are produced contribute to the EPOS4HQ single-particle spectra, which have already been compared with the experimental results in Ref. [14]. This is shown in Fig. 10, where we compare the EPOS4HQ results also with FONLL calculations [26,27] (shaded area). The p_T spectra at midrapidity for $\sqrt{s} = 5.02$ TeV are shown in the top row, with the p_T integrated rapidity distribution in the bottom row. In the left column, we display the results for charm quarks, and in the right column, those for bottom quarks. We see that for $p_T > 10$ GeV, the charm quarks from the gluon splitting process are dominant, whereas for bottom quarks, contributions from flavor creation are more important. Flavor excitation dominates both spectra at low p_T. The sum of all contributions is very similar to the FONLL prediction, for charm as well as for bottom quarks. The rapidity distributions are peaked at midrapidity and dominated due to the p_T integration by the flavor excitation process. In Fig. 11, we display the $D^0 + \bar{D}^0$ (left) and the $D^+ + D^-$ (right) spectra at midrapidity and forward rapidities. The different rows show different rapidity intervals: from central rapidities, measured by the ALICE Collaboration [54], to forward rapidities, measured by LHCb [55]. These are the underlying spectra for the correlation calculations presented in Fig. 7. We display as well the pure EPOS4 results. As explained in Ref. [14], all heavy mesons from EPOS4 are created by applying string decay; whereas in EPOS4HQ, a quark gluon plasma can be formed, and heavy quarks that emerge from this plasma can hadronize by coalescence. We see that the EPOS4 and EPOS4HQ calculations agree well with experiment. The differences are not visible in this logarithmic presentation. The rapidity spectra of EPOS4 and EPOS4HQ for the D mesons are shown in Fig. 12 as dashed and solid lines, respectively, in comparison with the FONLL calculations (shaded) and the experimental data. The deviation between theory and experiment comes exclusively from the difference in the p_T spectra at very low p_T, where pQCD-based calculations reach their natural limitations.

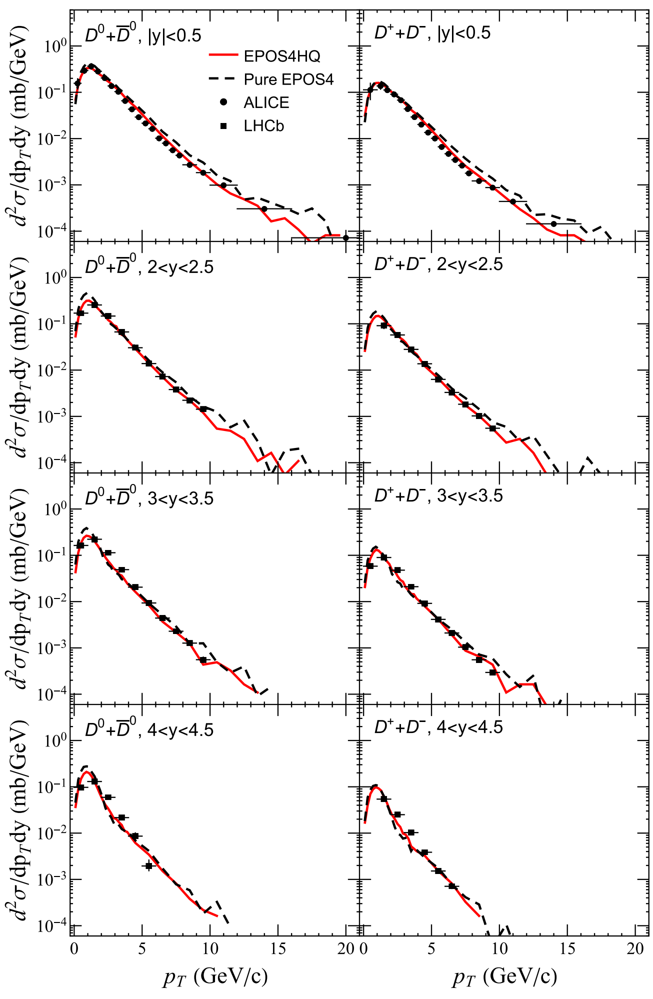

FIG. 11. p_T spectra of $D^0 + \bar{D}^0$ and $D^+ + D^-$ at central [−0.5, 0.5] and forward rapidity bins [2, 2.5], [3, 3.5], and [4, 4.5] in pp collisions at $\sqrt{s} = 5.02$ TeV. The experimental data are from ALICE [54] and LHCb [55].

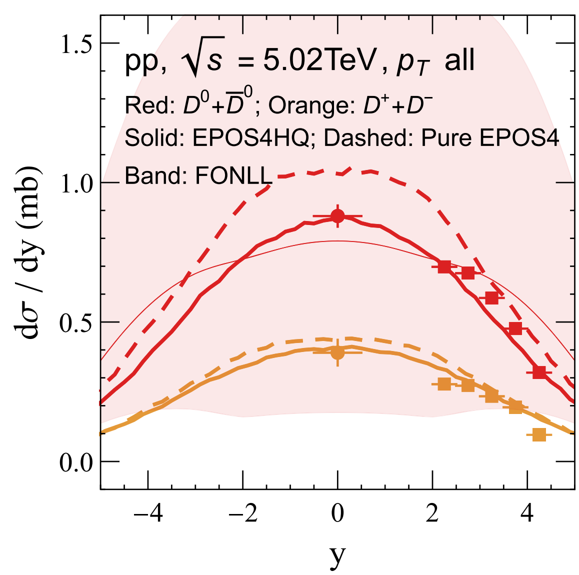

FIG. 12. Rapidity distribution of $D^0 + \bar{D}^0$ and $D^+ + D^-$ in pp collisions at $\sqrt{s} = 5.02$ TeV. The experimental data are from ALICE [54] and LHCb [55]. The band is the $D^0 + \bar{D}^0$ predicted by FONLL with the combined mass and scale uncertainties [26]. The thin solid line is the central value of the FONLL prediction.

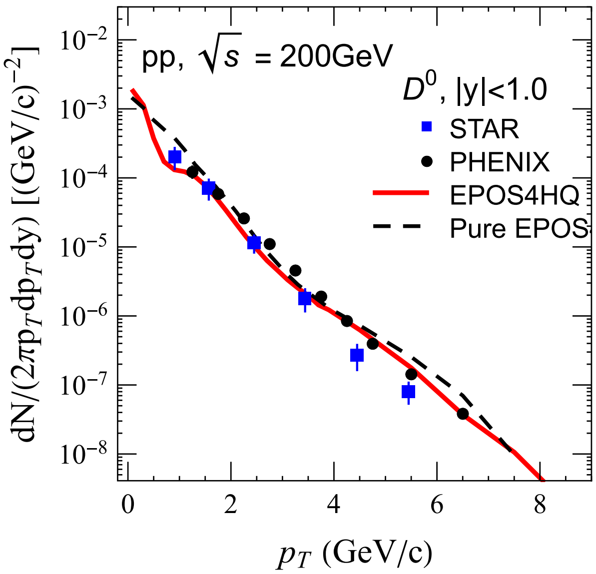

FIG. 13. p_T spectra of D^0 in the central rapidity bin, $|y| < 1.0$, of pp collisions at $\sqrt{s} = 200$ GeV. The experimental data are from STAR [56].

The p_T spectra of D^0 at top RHIC energy are shown in Fig. 13 and compared with the results of PHENIX and STAR. We see a good agreement. The lack of data at low p_T reduces the constraint of the low-p_T charm production, where the production is beyond the applicability of pQCD calculations. The spectra of D mesons are different in EPOS4 and EPOS4HQ due to the different hadronization mechanisms. In EPOS4, heavy hadrons are produced by fragmentation only, while in EPOS4HQ they can also be produced by coalescence. Hadronization by coalescence leads to an enhanced production of heavy baryons at low p_T, and hence to a reduction of the D mesons.

III. QUARKONIUM PRODUCTION

As said, the correlations between heavy quarks do not show up only in the correlation between open heavy flavor mesons, but influence as well the production of hidden heavy flavor mesons, because the probability that a Q and a $\bar{Q}$ form a quarkonium depends on their kinematic variables.

Before we investigate this in detail, we introduce our model for quarkonium production, which is based on the quantal density matrix approach, expressed in terms of Wigner densities. The idea to use a density matrix approach to study bound two-particle systems goes back to the seminal papers of Remler [57,58] and has recently been used to study quarkonium production in a thermal heat bath [59] and in heavy ion collisions [43]. In its time-independent form, this method has been widely applied in the so-called coalescence approach [60,61]. The density matrix approach to study quarkonia in pp collisions has been introduced in Refs. [42,44]. Here, we present an advanced version of this approach, which we discuss now in detail.

A. The density matrix approach

The density matrix formalism is based on the quantal density operators

$$\rho^{\Phi_i} = |\Phi_i\rangle\langle\Phi_i| \quad \text{and} \quad \rho^{Q\bar{Q}} = |Q\bar{Q}\rangle\langle Q\bar{Q}|, \tag{1}$$

where $\rho^{Q\bar{Q}}$ is the density matrix of the two-body $Q\bar{Q}$ system, and $|\Phi_i\rangle$ is the wave function of the ith quarkonium eigenstate. The production probability P_i of a quarkonium state Φ_i in a $Q\bar{Q}$ system can be described by their density operators ρ^{Φ_i} and $\rho^{Q\bar{Q}}$ via

$$P_i \equiv \mathrm{Tr}(\rho^{\Phi_i}\rho^{Q\bar{Q}}). \tag{2}$$

A density matrix ρ can be transformed into a Wigner density, which is defined as

$$\begin{aligned} W(\mathbf{x},\mathbf{q}) &= \int d^3y e^{-i\mathbf{q}\cdot\mathbf{y}/\hbar}\left\langle \mathbf{x}+\frac{\mathbf{y}}{2}|\rho|\mathbf{x}-\frac{\mathbf{y}}{2}\right\rangle \\ &= \int d^3y e^{-i\mathbf{q}\cdot\mathbf{y}/\hbar}\psi\left(\mathbf{x}-\frac{\mathbf{y}}{2}\right)\psi^*\left(\mathbf{x}+\frac{\mathbf{y}}{2}\right). \end{aligned} \tag{3}$$

The Wigner function satisfies the normalization condition,

$$\int \frac{d^3x d^3q}{(2\pi\hbar)^3} W(\mathbf{x},\mathbf{q}) = 1, \tag{4}$$

and reduces to

$$W(\mathbf{x},\mathbf{q}) = \delta(\mathbf{q}-\mathbf{q}_0), \tag{5}$$

if the particle is in a momentum eigenstate $\mathbf{q}_0$ and therefore described by a plane wave, $\psi(\mathbf{x}) = \frac{1}{\sqrt{(2\pi\hbar)^3}}e^{i\mathbf{q}_0\mathbf{x}}$. Introducing center-of-mass and relative coordinates

$$\begin{aligned} \mathbf{R} &= \frac{m_1\mathbf{r}_1 + m_2\mathbf{r}_2}{m_1+m_2}, \qquad \mathbf{r} = \mathbf{r}_1 - \mathbf{r}_2, \\ \mathbf{P} &= \mathbf{p}_1 + \mathbf{p}_2, \qquad \mathbf{p} = \frac{m_2\mathbf{p}_1 - m_1\mathbf{p}_2}{m_1+m_2}, \end{aligned} \tag{6}$$

we can transform the density matrix ρ^{Φ_i} into a Wigner density, which is defined as

$$\begin{aligned} W(\mathbf{R},\mathbf{P},\mathbf{r},\mathbf{p}) &= \int d^3y d^3Y e^{-i(\mathbf{p}\cdot\mathbf{y}+\mathbf{P}\cdot\mathbf{Y})/\hbar} \\ &\quad\times\left\langle \mathbf{R}+\frac{\mathbf{Y}}{2},\mathbf{r}+\frac{\mathbf{y}}{2}\middle|\rho^{\Phi_i}\middle|\mathbf{R}-\frac{\mathbf{Y}}{2},\mathbf{r}-\frac{\mathbf{y}}{2}\right\rangle \\ &= W^{\Phi_i}(\mathbf{r},\mathbf{p})\delta(\mathbf{P}-\mathbf{P}_0), \end{aligned} \tag{7}$$

assuming that the center-of-mass motion of the bound state i is described by a plane wave with momentum $\mathbf{P}_0$.

The Wigner density W^{Φ_i} of the quarkonium state Φ_i can be constructed via

$$W^{\Phi_i}(\mathbf{r},\mathbf{p}) = \int d^3y e^{-i\mathbf{p}\cdot\mathbf{y}}\psi_i\left(\mathbf{r}+\frac{\mathbf{y}}{2}\right)\psi_i^*\left(\mathbf{r}-\frac{\mathbf{y}}{2}\right). \quad (8)$$

Here, ψ_i is the wave function of quarkonium state i, which can be obtained by solving the Schrödinger equation for the relative coordinates of the $Q\bar{Q}$ pair. The momentum distribution of the center-of-mass motion of the quarkonium i, created in a system, which is in the quantum state $\rho^{Q\bar{Q}}$, is given by

$$\frac{dP_i}{d^3P} = g\int \frac{d^3Rd^3rd^3p}{(2\pi\hbar)^6}W^{\Phi_i}(\mathbf{r},\mathbf{p})W^{Q\bar{Q}}(\mathbf{R},\mathbf{P},\mathbf{r},\mathbf{p}) \times\delta(\mathbf{P}-\mathbf{P}_0). \quad (9)$$

In our semiclassical approach, we cannot calculate the quantal two-body Wigner density of a $Q\bar{Q}$ pair in the medium $W^{Q\bar{Q}}(\mathbf{R},\mathbf{P},\mathbf{r},\mathbf{p})$ directly. Like in all transport approaches, we average the classical phase-space density $W^{Q\bar{Q}}_{\text{class}}(\mathbf{R},\mathbf{P},\mathbf{r},\mathbf{p}) = dN^{Q\bar{Q}}/(d^3Rd^3Pd^3pd^3r)$, which is given by EPOS4, over many events.

The projection on the discrete quantum numbers like spin and color are encoded in a degeneracy factor g. $W^{Q\bar{Q}}_{\text{class}}$ contains all possibilities in spin $\otimes$ color space with the same probability. So, the degeneracy factor for a quarkonia with the total angular momentum J is $g = (2J+1)/(9\times 4)$, assuming color and spin are randomly distributed.

The extension to a system, which contains $N/2$ heavy quarks and $N/2$ heavy antiquarks (and hence $N^2/4$ pairs of $Q\bar{Q}$), mostly $c\bar{c}$ pairs, is straightforward. Summing over all $Q\bar{Q}$ pairs ik, we obtain

$$\begin{aligned}\frac{dP_{nl}}{d^3P} &= g\int d^3Rd^3rd^3pW^{\Phi}_{nl}(\mathbf{r},\mathbf{p})\\ &\times\sum_N\int\prod_{j=1}^N\frac{d^3r_jd^3p_j}{(2\pi\hbar)^3}W^{Q\bar{Q}}_{\text{class}}(\mathbf{r}_1,\mathbf{p}_1,\ldots,\mathbf{r}_N,\mathbf{p}_N)\\ &\times\sum_{\text{pairs}i,k}\delta\left(\frac{\mathbf{p}_i-\mathbf{p}_k}{2}-\mathbf{p}\right)\delta(\mathbf{r}_i-\mathbf{r}_k-\mathbf{r})\\ &\times\delta\left(\frac{\mathbf{r}_i+\mathbf{r}_k}{2}-\mathbf{R}\right)\delta(\mathbf{p}_i+\mathbf{p}_k-\mathbf{P})\delta(\mathbf{P}-\mathbf{P}_0), \quad (10)\end{aligned}$$

where $\mathbf{R}$, $\mathbf{P}$, $\mathbf{r}$, $\mathbf{p}$ are the center of mass and relative coordinates of the considered pair. We have introduced here the quantum numbers n and l of the state i. Both Eqs. (9) and (10) are nonrelativistic. For the relativistic version, which we apply in the calculations, we refer to Eq. (C9) in Appendix C of Ref. [43], where the details are given. In the relativistic version, one has to Lorentz-transform the momenta and positions of the heavy quarks, given by EPOS4 in the computational frame, into the center-of-mass system of the $Q\bar{Q}$ pair and determines there the probability[2] $W^{\Phi}_{nl}(\mathbf{r}_{cm},\mathbf{p}_{cm})$ that this pair is in a state Φ_i. In the computational frame, the momentum distribution is then given by [43]

$$\frac{dP_{nl}}{d^3P} = \left\langle g\sum_{Q\bar{Q}\,\text{pairs}}W^{\Phi}_{nl}(\mathbf{r}_{cm},\mathbf{p}_{cm})\delta^{(3)}(\mathbf{P}-\mathbf{p}_1-\mathbf{p}_2)\right\rangle, \quad (11)$$

where the summation runs over all $N^2/4$ possible $Q\bar{Q}$ pairs, and where $\mathbf{r}_{cm}$ and $\mathbf{p}_{cm}$ are the relative distance and momentum in the center-of-mass frame of each $Q\bar{Q}$ pair. The set of angle brackets $\langle\cdots\rangle$ indicates the averaging over all Monte Carlo events generated by EPOS4. In the minimum-bias pp collisions at 200 GeV and 5.02 TeV, the production of a quarkonium state predominantly proceeds via the hadronization of a single $Q\bar{Q}$ pair created in the same parton interaction. While EPOS4 allows for the production of multiple independent $Q\bar{Q}$ pairs via multiparton interactions, the contribution from the different-pair recombination (where a quark from one pair binds with an antiquark from another) to be subleading at the collision energies and multiplicities studied in this paper. A detailed study of recombination effects in high-multiplicity events at higher energies (e.g., 13 TeV) is left for future work.

We come now to the construction of the quarkonium Wigner function W^{Φ}_{nl}. The Wigner function is obtained from the quarkonium wave function via a Wigner transformation, and the wave function is the solution of the two-body Schrödinger equation. In our approach, the nonrelativistic approximation is applied to the internal wave function of the heavy quark-antiquark pair in its rest frame, while the total momentum of the pair is treated fully relativistically. Since the relevant expansion parameter is the relative velocity $v \ll 1$, the use of a nonrelativistic description for the bound state is well justified. Consequently, employing a nonrelativistic bound-state wave function remains theoretically consistent within the expected power-counting scheme. The interaction potential can be taken as Cornell potential in vacuum, $V(r) = -\alpha/|\mathbf{r}| + \sigma|\mathbf{r}|$, with $\alpha = 0.513$ and $\sigma = 0.17\ \text{GeV}^2$, and the quark mass $m_c = 1.5$ GeV, $m_b = 5.2$ GeV. Because the potential depends only on the relative distance of two quarks, we can separate the motion of the two-body system into a center-of-mass motion, which is just the motion of a free particle, and the relative motion. Furthermore, the Cornell potential is an isotropic potential. One can write the relative wave function $\psi(\mathbf{r})$ into a radial part and an angular part, $\psi(\mathbf{r}) = R_{nl}(r)Y_{l,m}(\theta,\phi)$. Now, the

[2]Strictly speaking, in Eq. (C8) of Ref. [43], the quarkonium is assumed to have the same 4-velocity as the $c\bar{c}$ pair, while the invariant mass is assumed to be modified. By contrast, here momentum conservation is assumed and energy conservation is violated. This difference should not modify the result in a noticeable way.

description of the two-body system is simplified to a one-dimensional problem:

$$\left[-\frac{1}{2\mu}\left(\frac{d^2}{dr^2}+\frac{2}{2}\frac{d}{dr}\right)+\frac{l(l+1)}{2\mu r^2}+V(r)\right]R_{nl}(r)=ER_{nl}(r), \tag{12}$$

where $\mu = m_i m_j/(m_i + m_j)$ is the reduced mass. Here, (n, l) labels the main and orbital angular momentum number of quarkonium states. We solve the two-body Schrödinger equation for charmonium, bottomonium, and B_c. The wave functions are shown in Fig. 14, and the masses and root-mean-square (rms) radii $\langle r^2\rangle$ are shown in Table I. We can see that the masses are very close to the experimental values. However, the wave function is not analytical, and therefore the calculation of the Wigner density and of Eq. (8) can only be performed numerically. To avoid this, we assume that the potential between the heavy quark pairs can be approximated by a 3D isotropic harmonic oscillator (HO) potential, $V(r) = 1/(2m_Q\sigma^4)r^2$. Then, the wave functions are analytical. The wave functions of a 3D isotropic harmonic oscillator can be expressed as $\psi_{nlm}(r,\theta,\phi) = R_{nl}(r)Y_{l,m}(\theta,\phi)$, where $Y_{l,m}$ are the spherical harmonics. The radial part can be expressed as

$$R_{nl}(r)=\left[\frac{2(n!)}{\sigma^3\Gamma(n+l+3/2)}\right]^{\frac{1}{2}}\left(\frac{r}{\sigma}\right)^l e^{-\frac{r^2}{2\sigma^2}}L_n^{l+1/2}\left(\frac{r^2}{\sigma^2}\right), \tag{13}$$

where $L_n^{l+1/2}$ are the Laguerre polynomials. The width σ of the harmonic oscillator potential is chosen such that the numerically determined rms radius of the eigenfunction of the Cornell potential, tabulated in Table I, agrees with that of the harmonic oscillator potential. The rms radii of the different harmonic oscillator wave functions are related to the widths of these states by $\langle r^2\rangle = 3\sigma^2/2$ for $1S$, $\langle r^2\rangle = 5\sigma^2/2$ for $1P$, $\langle r^2\rangle = 7\sigma^2/2$ for $1D$ and $2S$, $\langle r^2\rangle = 9\sigma^2/2$ for $2P$, and $\langle r^2\rangle = 11\sigma^2/2$ for the $3S$ state. This procedure allows us to connect the 3D isotropic harmonic oscillator wave function with the real quarkonium wave function via the rms radii $\langle r^2\rangle$. The related widths are shown in Table I, and the wave functions are shown in Fig. 14 as dashed lines. We can see that the ground state and the low excited states can be well reproduced by the 3D isotropic harmonic oscillator, while the differences for higher-order excited states—e.g., $2S$, $2P$, and $3S$—are larger.

With this analytical wave function, the Wigner function can be constructed via a Wigner transformation in spherical coordinates. The Wigner function for any given (n, l) state, including the summation on all harmonics m, can be expressed as

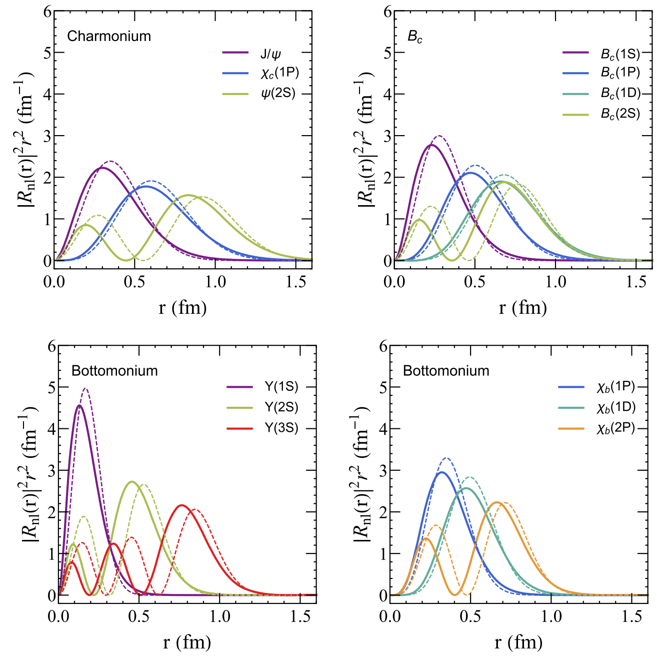

FIG. 14. Wave function of different charmonium (upper), B_c (middle), and bottomonium (lower) states. Solid lines are from the Schrödinger equation, while dashed lines are from the 3D isotropic harmonic oscillator and given by Eq. (13).

$$\begin{aligned} W_{nl}^{\Phi}(\mathbf{r},\mathbf{p}) &= \frac{1}{2l+1}\frac{(-1)^l}{2\pi^3}\sum_{n'+N+l'=K}(-1)^{n'+3l'/2} \\ &\times\sqrt{\frac{\pi(2l+1)(2l'+1)n'!N!}{\Gamma(n'+l'+3/2)\Gamma(N+l'+3/2)}} \\ &\times(n'l'Nl'0|nlnl0)L_N^{l'+1/2}(2\mathbf{r}^2)L_N^{l'+1/2}(2\mathbf{p}^2) \\ &\times(2\|\mathbf{r}\|\|\mathbf{p}\|)^{l'}P_{l'}(\cos\theta)e^{-(\mathbf{r}^2+\mathbf{p}^2)}, \end{aligned} \tag{14}$$

TABLE I. The masses, root-mean-square radius, and Gaussian widths σ of different charmonium and bottomonium states in vacuum. The experimental data for the masses are from Ref. [62].

States	M_{Theo}(GeV)	M_{Exp}(GeV)	$\langle r^2\rangle$(fm^2)	σ(fm)
J/ψ	3.071	3.097	0.182	0.348
$\chi_c(1P)$	3.483	3.463	0.453	0.426
$\psi(2S)$	3.652	3.686	0.714	0.452
$\Upsilon(1S)$	9.390	9.460	0.042	0.167
$\chi_b(1P)$	9.870	9.876	0.153	0.247
$\chi_b(1D)$	10.109	10.163	0.284	0.285
$\Upsilon(2S)$	9.959	10.023	0.236	0.260
$\chi_b(2P)$	10.208	10.243	0.410	0.302
$\Upsilon(3S)$	10.288	10.355	0.520	0.307
$B_c(1S)$	6.482	6.275	0.115	0.277
$B_c(1P)$	6.895	⋯	0.316	0.356
$B_c(1D)$	7.156	⋯	0.542	0.393
$B_c(2S)$	7.033	6.872	0.497	0.377

where $K = 2n + l$. The summation is from zero to K, and for all possible quantum numbers n', l', and N. The only restriction on these quantum numbers is that the sum is K. The value θ is the angle between $\mathbf{r}$ and $\mathbf{p}$, L_n^l are the generalized Laguerre polynomials, $P_{l'}$ are the Legendre polynomials, and $(n'l'Nl'0|nlnl0)$ is the Talmi-Brody-Moshinsky (TBM) bracket. This expression has first been given in Ref. [63], to which we refer for the details.

For the states up to $3S$, the Wigner densities have the concrete form

$$\begin{aligned}
W^{\Phi}_{1\mathrm{S}}(\mathbf{r},\mathbf{p}) &= 8e^{-\xi},\\
W^{\Phi}_{1\mathrm{P}}(\mathbf{r},\mathbf{p}) &= \frac{8}{3}e^{-\xi}(2\xi-3),\\
W^{\Phi}_{1\mathrm{D}}(\mathbf{r},\mathbf{p}) &= \frac{8}{15}e^{-\xi}(15+4\xi^2-20\xi+8[p^2r^2-(\mathbf{p}\cdot\mathbf{r})^2]),\\
W^{\Phi}_{2\mathrm{S}}(\mathbf{r},\mathbf{p}) &= \frac{8}{3}e^{-\xi}(3+2\xi^2-4\xi-8[p^2r^2-(\mathbf{p}\cdot\mathbf{r})^2)]),\\
W^{\Phi}_{2\mathrm{P}}(\mathbf{r},\mathbf{p}) &= \frac{8}{15}e^{-\xi}(-15+4\xi^3-22\xi^2+30\xi-8(2\xi-7)[p^2r^2-(\mathbf{p}\cdot\mathbf{r})^2]),\\
W^{\Phi}_{3\mathrm{S}}(\mathbf{r},\mathbf{p}) &= \frac{8}{315}e^{-\xi}(315+42\xi^4-336\xi^3+924\xi^2-840\xi\\
&\quad -[2009+32p^2r^2+336r^4/\sigma^4-1400r^2/\sigma^2-896p^2\sigma^2+224p^4\sigma^4][p^2r^2-(\mathbf{p}\cdot\mathbf{r})^2]\\
&\quad -[686+608p^2r^2+112r^2/\sigma^2-896p^2\sigma^2+224p^4\sigma^4-672(\mathbf{p}\cdot\mathbf{r})^2](\mathbf{p}\cdot\mathbf{r})^2), \qquad (15)
\end{aligned}$$

where $\xi = \frac{r^2}{\sigma^2} + p^2\sigma^2$. We can see that the Wigner densities of the excited states depend not only on $r = |\mathbf{r}|$ and $p = |\mathbf{p}|$, but also on the angle between $\mathbf{p}$ and $\mathbf{r}$.

In EPOS4, the Q and $\bar{Q}$ are produced at the same position in coordinate space with the momenta $\mathbf{p}_1$ and $\mathbf{p}_2$. The Wigner density $W^{\Phi}_{nl}(\mathbf{r},\mathbf{p})$ can be locally negative, but all differential rates should be positive if the integration is performed over an elementary phase-space cell h^3. To avoid negative probabilities and restore the compatibility with the Heisenberg principle, we sample the relative distance $\mathbf{r}_{cm}$ between Q and $\bar{Q}$ in their center-of-mass frame by a Gaussian distribution around the EPOS4 production point of the pair,

$$f(\mathbf{r}_{cm}) \sim r_{cm}^2 \exp\left(-\frac{r_{cm}^2}{2\sigma^2_{\mathrm{Q\bar{Q}}}}\right), \qquad (16)$$

where the relative distance is controlled by the effective width $\sigma_{\mathrm{Q\bar{Q}}}$, which is $\sigma_{c\bar{c}} = 0.35$ fm for all charmonium states (as this parameter enters only the $W^{c\bar{c}}$ distribution) and $\sigma_{b\bar{b}} = 0.2$ fm for all bottomonium states.

We can now calculate Eq. (11) for all charmonium and bottomonium states, as well for B_c, by averaging over many EPOS4HQ events. Because in this microscopic approach we follow all heavy quarks individually (and not only their distribution function), we can trace back the origin of all heavy quarks, which are finally entrained in quarkonia states. Table II presents the percentage distribution of the creation processes for the final D^0, J/ψ, B^0, and $\Upsilon(1S)$ mesons. We observe that the gluon splitting contribution is, as expected in a Wigner projection approach, more important for the quarkonia than for the open heavy flavor mesons, whereas for flavor creation the opposite is the case, due to the unfavorable kinematics. If we introduce a lower-p_T cut, the influence of the flavor excitation process becomes smaller.

TABLE II. The fractions of D^0 (B^0) and prompt J/ψ [$\Upsilon(1S)$] from different processes.

Fraction	Flavor creation	Flavor excitation	Gluon splitting
D^0	6.12%	80.63%	13.25%
J/ψ	2.62%	76.02%	21.36%
B^0	26.96%	65.72%	7.32%
$\Upsilon(1S)$	11.56%	73.20%	15.24%

B. Quarkonia observables

In Fig. 15, we display the p_T distribution at midrapidity (left), as well as the p_T integrated rapidity distribution (right) of the different quarkonia. The top figures show the distributions for the charmonia, followed by those for bottomonia, for χ_b, and for B_c. The slopes of the p_T spectra are rather different for charmonia, bottomonia, and B_c; the rapidity distributions show a small double-hump structure for charmonia and a rather flat distribution around midrapidity for bottomonia and B_c.

The comparison of the EPOS4HQ calculations with the presently available charmonium data at $\sqrt{s} = 5.02$ TeV is

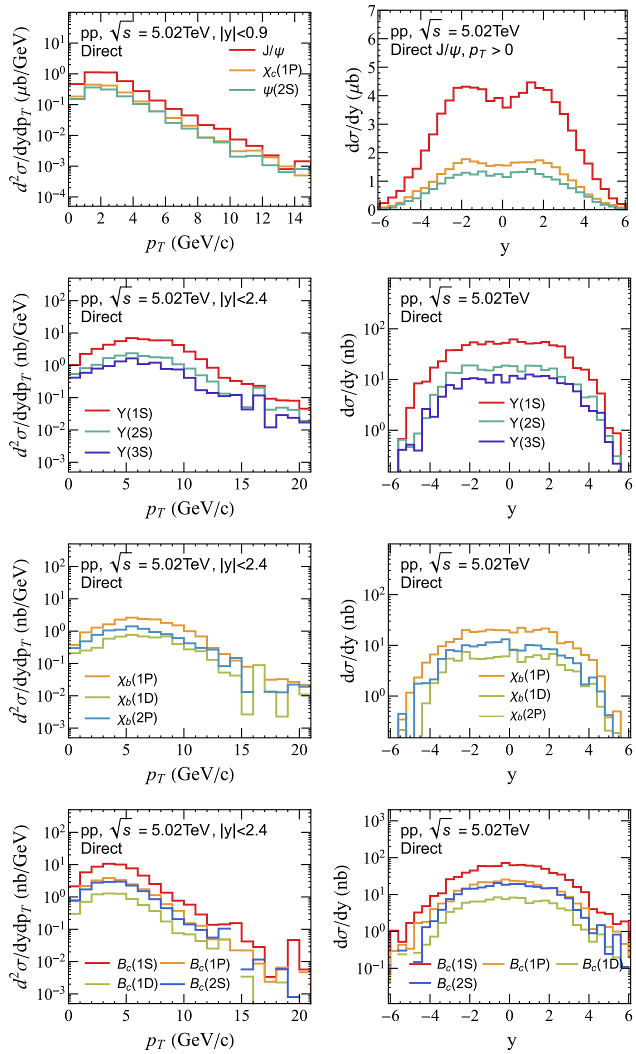

FIG. 15. p_T spectra at midrapidity and the rapidity distribution of different directly produced charmonium states [upper], bottomonium states [middle for S-wave and $P(D)$-wave], and B_c states [lower] in pp collisions at $\sqrt{s} = 5.02$ TeV. The color-coding of the different states is noted in the figure.

shown in Fig. 16. The top figures display the p_T spectra for prompt J/ψ at midrapidity and the p_T integrated rapidity distribution, while the bottom figures show the results for the prompt $\psi(2S)$, where experimentally only a transverse momentum spectrum is available. The prompt J/ψ is the summation of the direct produced J/ψ and the feed-down from the χ_c and $\psi(2S)$ to J/ψ with the branching ratios 30% and 61%, respectively. We show the contributions from the different $Q\bar{Q}$ production processes, as well as the sum. The color-coding is that of Fig. 4. We see that quarkonia with $p_T > 4$ GeV are almost exclusively produced by heavy quarks, which originate from the gluon splitting process in which the $Q\bar{Q}$ have a small azimuthal opening angle, favorable for the production of a charmonium. Only at very low p_T is flavor excitation dominant, and flavor creation contributes only marginally to the

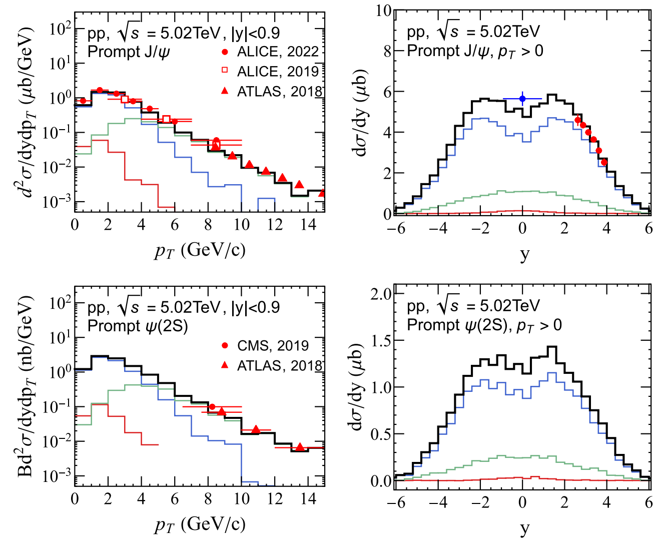

FIG. 16. p_T spectra and rapidity distribution of prompt J/ψ (upper) and $\psi(2S)$ (lower) (thick black lines) in pp collisions at $\sqrt{s} = 5.02$ TeV. Red is the contribution from flavor creation, blue that from flavor excitation, and green from gluon splitting. The experimental data are from ALICE [64,65], ATLAS [66], and CMS [67]. The branching ratio of $B(\psi(2S) \to \mu^+\mu^-)$ is taken as 0.8%, as given by the PDG [62].

charmonium p_T spectra. Figure 17 shows the influence of the $Q\bar{Q}$ correlations on the prompt J/ψ transverse momentum distribution. Here, we compare the spectrum with the correlations (black line) and the spectrum where we have randomized the azimuthal distributions between the $Q\bar{Q}$ pair. This randomization mostly affects the gluon splitting process, where the $Q\bar{Q}$ are strongly correlated, and which is dominant at high p_T. We see a visible modification of the slope, which is p_T-dependent, because the different pQCD creation processes depend differently on p_T.

The spectra at the highest RHIC energy are shown in Fig. 18 for J/ψ (top row) and for $\psi(2s)$ (bottom row). On the left-hand side, we display the p_T spectra; on the right-hand side, we show the rapidity distribution. Our calculations are compared with PHENIX [68] and STAR [69] data. A good agreement between the EPOS4HQ and J/ψ data for almost all p_T is found.

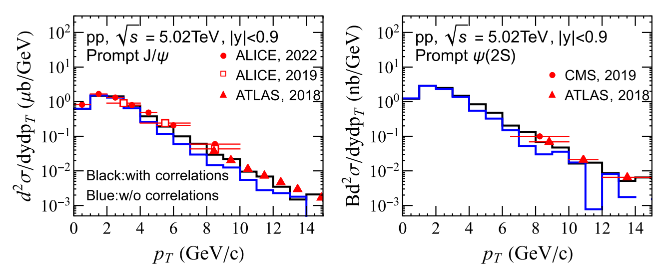

FIG. 17. p_T spectra of prompt J/ψ and $\psi(2S)$. The blue lines are obtained with the same framework and parameters, but assuming that the correlations between c and $\bar{c}$ are random.

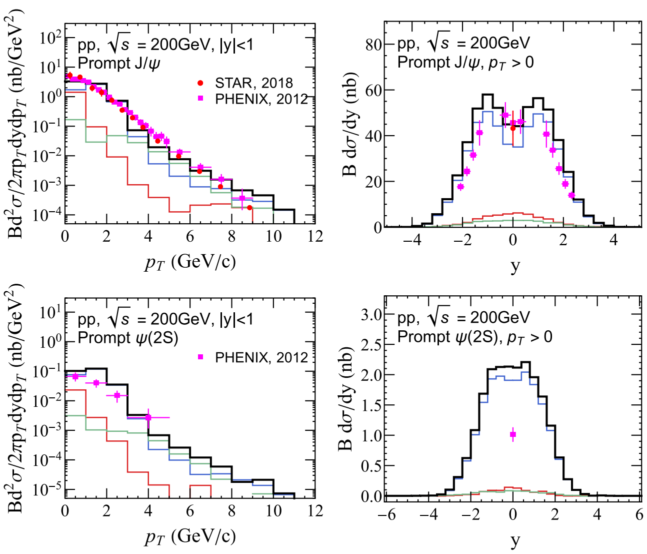

FIG. 18. p_T spectra and rapidity distribution of prompt J/ψ (upper) and $\psi(2S)$ (lower) (thick black lines) in pp collisions at $\sqrt{s} = 200$ GeV. Red is the contribution from flavor creation, blue that from flavor excitation, and green from gluon splitting. The experimental data are from PHENIX [68] and STAR [69].

The p_T distribution of $\psi(2s)$ is slightly overpredicted. We display in this figure as well the spectra of the different production processes of the c quarks. All spectra are dominated by creation via the flavor excitation process. Flavor creation does not play a role at all, whereas gluon splitting contributes modestly at high p_T.

Figure 19 shows the p_T distribution at midrapidity (left) as well the p_T integrated rapidity distribution (right) of the different prompt bottomonia in comparison with experimental data, when available. The prompt $\Upsilon(nS)$ comes from direct production and the feed-down from the excited states. In this study, we take the branching ratios 23%, 20%, 7%, 7%, and 1% for $\chi_b(1P)$, $\chi_b(1D)$, $\Upsilon(2S)$, $\chi_b(2P)$, and $\Upsilon(3S)$, respectively, to the ground state $\Upsilon(1S)$; we take 9.3% and 10.6% for $\chi_b(2P)$ and $\Upsilon(3S)$, respectively, to $\Upsilon(2S)$, as suggested by PDG [62]. From top to bottom, we display the spectra for prompt $\Upsilon(1S)$, $\Upsilon(2S)$, and $\Upsilon(3S)$. Also here, the bottomonia with a high transverse momentum stem from bottom quarks produced by gluon splitting, in contradistinction to the B-meson spectrum (Fig. 10). This is dominated by b quarks coming from flavor creation, which contribute very little to the production of bottomonia. The EPOS4HQ results agree within the error bars with the experimental results for all bottomonia states.

We note that, in a fully relativistic treatment, the boost to the pair center-of-mass frame induces a time difference between the heavy quark and antiquark due to the relativity of simultaneity, as shown in Eq. (11). This time shift increases with the Lorentz factor of the pair and therefore becomes more pronounced at large total transverse momentum. However, its numerical impact is suppressed by the

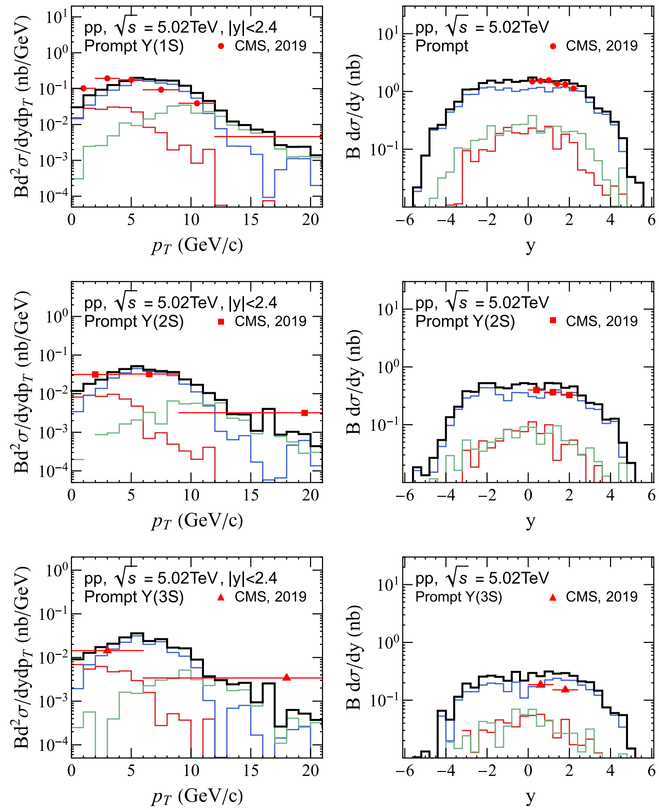

FIG. 19. p_T spectra and rapidity y dependence of prompt $\Upsilon(1S)$ (upper), $\Upsilon(2S)$ (middle), and $\Upsilon(3S)$ (lower) (thick black lines). Red is the contribution from flavor creation, blue that from flavor excitation, and green from gluon splitting. The experimental data are from CMS [70]. The branching ratios of $B(\Upsilon(nS) \to \mu^+\mu^-)$ are taken as 2.48% for $1S$, 1.93% for $2S$, and 2.18% for $3S$, which are given by PDG [62].

small spatial size of quarkonia and the moderate boost of bottomonium in the kinematic range considered here, rendering the effect negligible for $p_T < 20$ GeV. For charmonium, the effect remains under control and does not significantly affect our results for $p_T < 10$ GeV, which is the kinematic region relevant for our phenomenological analysis.

C. B_c production

We come now to the production of B_c mesons. In heavy ion collisions at low p_T, the creation of a significant yield of B_c mesons is considered as a witness that a QGP is created [71] with which the heavy quarks interact and where the B_c is finally formed by hadronization. In pp collisions, since the bottom and charm quarks cannot be produced at the same vertex and a production due to hadronic scattering is very improbable, it can only appear in the rare pp collisions in which a $c\bar{c}$ and a $b\bar{b}$ pair are created in the same pp collision—they may be produced from the same Pomeron [62] or from two different Pomerons. EPOS4HQ calculations show that the latter process is dominant. It is therefore

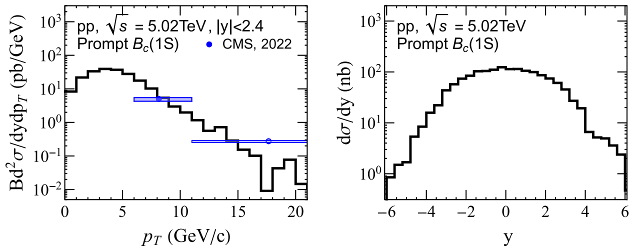

FIG. 20. p_T spectrum and rapidity y dependence of the prompt $B_c(1S)$ state. The experimental data are from CMS [71]. The branching ratio is $B(B_c^+ \to (J/\psi \to \mu^+\mu^-)\mu^+ v_\mu)$.

interesting to study the B_c yield in pp, where an eventually produced QGP does not modify the B_c spectra substantially, not only to understand better the spatial structure of the interaction zone, but also to provide a reference point for the comparison with heavy ion collisions.

In Fig. 20, we display the EPOS4HQ results for the transverse momentum spectrum of the B_c at midrapidity (left) and their rapidity distribution (right). The transverse momentum distribution is compared with CMS data. The experimental data are displayed with the branching ratio $B(B_c \to (J/\psi \to \mu^+\mu^-)\mu^+ v_\mu)$, where $B(J/\psi \to \mu^+\mu^-) = 5.96\%$ for J/ψ is given by PDG [62]. However, the decay branching ratio $B(B_c \to J/\psi\mu^+ v_\mu)$ has not been observed in experiments. There are many theoretical predictions, which give a uncertainty range of 1.2% to 6.7% [72–74]. In our study, we find that the spectrum can be well described by taking almost the central value of $B(B_c \to J/\psi\mu^+ v_\mu) = 3.5\%$. Due to the lack of information about the decay of the excited states, we take 100% as the branching ratio for all excited states to the ground state B_s. As said, the $\bar{b}$ and the c quark cannot come from the same vertex. A detailed investigation shows that they almost never come from the same Pomeron, so B_c is only produced when at least two Pomerons are exchanged between the two incoming protons. It is remarkable that with a source parameter $\sigma_{c\bar{b}} = \sqrt{(\sigma_{c\bar{c}}^2 + \sigma_{b\bar{b}}^2)/2} = 0.285$ fm, which controls the distance between b and c sources, we can also reproduce the B_c using Eq. (11). In view of the fact that the heavy quarks in a B_c come from different vertices, and despite of the uncertainties of the branching ratio, this is an indication that EPOS4HQ describes reasonably not only the momentum-space observables but also the coordinate-space distribution of the vertices.

TABLE III. The origin of the heavy mesons entrained in B_c mesons. We present the percentage distribution for the different heavy quark production processes. P1 is flavor creation, P2 is flavor excitation, and P3 is gluon splitting.

Fraction	$\bar{b}$ from P1	$\bar{b}$ from P2	$\bar{b}$ from P3
c from P1	2.48%	4.42%	0.32%
c from P2	17.66%	61.20%	5.68%
c from P3	2.56%	5.25%	0.43%

TABLE IV. Expected percentage distribution of the origin of heavy quarks, entrained in B_c mesons, if the production of both heavy quarks are uncorrelated (see text).

Fraction	$\bar{b}$ from P1	$\bar{b}$ from P2	$\bar{b}$ from P3
c from P1	1.64%	5.12%	0.46%
c from P2	19.19%	59.91%	5.44%
c from P3	1.87%	5.84%	0.53%

The origin of heavy quarks, entrained in a B_c, is shown in Table III. For the majority of B_c, both heavy quarks come from flavor excitation processes. Since the $b\bar{b}$ and $c\bar{c}$ stem from independent processes, one would expect that each entry of Table III can be written as $\mathrm{prob}(c)_i \times \mathrm{prob}(\bar{b})_j$, where $\mathrm{prob}(c)_i$ and $\mathrm{prob}(\bar{b})_j$ are the cumulated distribution corresponding to Table III: namely, $\mathrm{prob}(\bar{b}) = \{22.70\%, 70.87\%, 6.43\%\}$ and $\mathrm{prob}(c) = \{7.22\%, 84.54\%, 8.24\%\}$. The corresponding results are displayed in Table IV. One sees that they are indeed close to those of Table III, with small differences in the last column, which tends to confirm the independent production hypothesis.

IV. SUMMARY

In summary, we have investigated the influence of different pQCD processes for heavy flavor production on heavy flavor meson observables in pp collisions at RHIC and LHC energies. The different azimuthal correlations of these processes show up in the correlations between open heavy flavor mesons, as well as in the production of quarkonia.

We have verified that EPOS4HQ reproduces well the measured open heavy flavor meson spectra, as well as the (different) correlations between $D\bar{D}$ and $B\bar{B}$ mesons. We have analyzed the influence of the different ways in which heavy quark pairs are produced on these correlations and have shown that the form of these correlations can be well identified with the different production processes, whose weight is different for D and B mesons. It turns out that flavor excitation is the dominant process of heavy quark production. At high p_T, flavor creation and gluon splitting also contribute differently for b and c quarks. This shows that the production of heavy mesons cannot be described by simplified models which use parton distribution and fragmentation functions only.

The charmonium and bottomonium production in high-energy pp collisions is described via the Wigner density approach based on the eigenfunctions of the Schrödinger equation of the different quarkonia states. Here, we have included all states up to $3S$ states. The similarity of the eigenfunctions and the harmonic oscillator wave functions shows that the eigenfunctions are essentially characterized by the root-mean-square distance between the heavy quark and its antiquark, which is different for $c\bar{c}$ and $b\bar{b}$ pairs. With this one parameter, all excited states can be calculated, and the results show a good agreement with experimental data.

The correlations between heavy quarks play an important role for the quarkonia observables. The three types of production contribute quite differently to the p_T spectra of quarkonia, and only the sum of them creates agreement with experiment. Therefore, for the production of quarkonia, the correlations between the quark and antiquark in the different productions and the relative contributions of the different processes are essential.

Finally, we have shown that the same density matrix approach, without any additional parameter, also allows us to reproduce quantitatively the experimental p_T spectra of B_c mesons, which are formed by heavy quarks coming from different Pomerons, although the uncertainty of the branching ratio is large. This confirms that the spatial quark distribution in the interaction zone of a pp collision is described by the prescription adopted in the EPOS4HQ approach. Future progress on the spatial distribution of partons in hadrons will be helpful to impose more constraints on these parameters.

ACKNOWLEDGMENTS

We thank E. Bratkovskaya and T. Song for fruitful discussions. This work is funded by the European Union's Horizon 2020 research and innovation program under Grant Agreement No. 824093 (STRONG-2020). J. X. is also support by the Helmholtz Research Academy Hessen for FAIR (HFHF).

DATA AVAILABILITY

The data come from the EPOS4 simulation code. We have released the new version of EPOS4, which anyone can download to perform related simulations.

[1] H. van Hees, V. Greco, and R. Rapp, Phys. Rev. C **73**, 034913 (2006).
[2] M. He, R. J. Fries, and R. Rapp, Phys. Rev. C **86**, 014903 (2012).
[3] V. Minissale, S. Plumari, and V. Greco, Phys. Lett. B **821**, 136622 (2021).
[4] S. Cao, G.-Y. Qin, and S. A. Bass, Phys. Rev. C **92**, 024907 (2015).
[5] S. Cao, T. Luo, G.-Y. Qin, and X.-N. Wang, Phys. Rev. C **94**, 014909 (2016).
[6] S. Cao *et al.*, Phys. Rev. C **99**, 054907 (2019).
[7] S. Cao, K.-J. Sun, S.-Q. Li, S. Y. F. Liu, W.-J. Xing, G.-Y. Qin, and C. M. Ko, Phys. Lett. B **807**, 135561 (2020).
[8] P. B. Gossiaux, R. Bierkandt, and J. Aichelin, Phys. Rev. C **79**, 044906 (2009).
[9] T. Song, H. Berrehrah, D. Cabrera, J. M. Torres-Rincon, L. Tolos, W. Cassing, and E. Bratkovskaya, Phys. Rev. C **92**, 014910 (2015).
[10] T. Song, H. Berrehrah, D. Cabrera, W. Cassing, and E. Bratkovskaya, Phys. Rev. C **93**, 034906 (2016).
[11] M. He and R. Rapp, Phys. Rev. Lett. **124**, 042301 (2020).
[12] H. T. Li, Z. L. Liu, and I. Vitev, Phys. Lett. B **816**, 136261 (2021).
[13] A. Beraudo, A. De Pace, M. Monteno, M. Nardi, and F. Prino, Eur. Phys. J. C **82**, 607 (2022).
[14] J. Zhao, J. Aichelin, P. B. Gossiaux, V. Ozvenchuk, and K. Werner, Phys. Rev. C **110**, 024909 (2024).
[15] L. Adamczyk*et al.* (STAR Collaboration), Phys. Rev. Lett. **118**, 212301 (2017).
[16] J. Adam *et al.* (STAR Collaboration), Phys. Rev. C **99**, 034908 (2019).
[17] S. Acharya *et al.* (ALICE Collaboration), J. High Energy Phys. 01 (2022) 174.
[18] S. Acharya *et al.* (ALICE Collaboration), Phys. Lett. B **813**, 136054 (2021).
[19] A. M. Sirunyan *et al.* (CMS Collaboration), Phys. Lett. B **816**, 136253 (2021).
[20] A. M. Sirunyan *et al.* (CMS Collaboration), Phys. Lett. B **782**, 474 (2018).
[21] R. Aaij *et al.* (LHCb Collaboration), J. High Energy Phys. 06 (2012) 141; 03 (2014) 108(A).
[22] J. Adam *et al.* (STAR Collaboration), Phys. Lett. B **797**, 134917 (2019).
[23] B. B. Abelev *et al.* (ALICE Collaboration), Phys. Lett. B **734**, 314 (2014).
[24] S. Acharya *et al.* (ALICE Collaboration), J. High Energy Phys. 10 (2020) 141.
[25] L. Adamczyk *et al.* (STAR Collaboration), Phys. Rev. Lett. **111**, 052301 (2013).
[26] M. Cacciari, M. Greco, and P. Nason, J. High Energy Phys. 05 (1998) 007.
[27] M. Cacciari, P. Nason, and R. Vogt, Phys. Rev. Lett. **95**, 122001 (2005).
[28] E. Norrbin and T. Sjostrand, Eur. Phys. J. C **17**, 137 (2000).
[29] R. Vogt, Phys. Rev. C **98**, 034907 (2018).
[30] D. Souza and N. H. Brook, J. Phys. G **43**, 015001 (2016).
[31] R. Maciula and A. Szczurek, EPJ Web Conf. **81**, 01007 (2014).
[32] H. Fritzsch, Phys. Lett. **67B**, 217 (1977).
[33] J. F. Amundson, O. J. P. Eboli, E. M. Gregores, and F. Halzen, Phys. Lett. B **372**, 127 (1996).
[34] V. Cheung and R. Vogt, Phys. Rev. D **98**, 114029 (2018).
[35] C.-H. Chang, Nucl. Phys. **B172**, 425 (1980).
[36] R. Baier and R. Ruckl, Phys. Lett. **102B**, 364 (1981).
[37] G. T. Bodwin, E. Braaten, T. C. Yuan, and G. P. Lepage, Phys. Rev. D **46**, R3703 (1992).

[38] G. T. Bodwin, E. Braaten, and G. P. Lepage, Phys. Rev. D **51**, 1125 (1995); **55**, 5853(E) (1997).

[39] M. Butenschoen and B. A. Kniehl, Phys. Rev. Lett. **108**, 172002 (2012).

[40] B. Gong, L.-P. Wan, J.-X. Wang, and H.-F. Zhang, Phys. Rev. Lett. **110**, 042002 (2013).

[41] K.-T. Chao, Y.-Q. Ma, H.-S. Shao, K. Wang, and Y.-J. Zhang, Phys. Rev. Lett. **108**, 242004 (2012).

[42] T. Song, J. Aichelin, and E. Bratkovskaya, Phys. Rev. C **96**, 014907 (2017).

[43] D. Y. A. Villar, J. Zhao, J. Aichelin, and P. B. Gossiaux, Phys. Rev. C **107**, 054913 (2023).

[44] T. Song, J. Aichelin, J. Zhao, P. B. Gossiaux, and E. Bratkovskaya, Phys. Rev. C **108**, 054908 (2023).

[45] K. Werner, Phys. Rev. C **108**, 064903 (2023).

[46] K. Werner and B. Guiot, Phys. Rev. C **108**, 034904 (2023).

[47] K. Werner, Phys. Rev. C **109**, 034918 (2024).

[48] K. Werner, Phys. Rev. C **109**, 014910 (2024).

[49] J. Zhao, J. Aichelin, P. B. Gossiaux, and K. Werner, Phys. Rev. D **109**, 054011 (2024).

[50] T. Sjöstrand, S. Ask, J. R. Christiansen, R. Corke, N. Desai, P. Ilten, S. Mrenna, S. Prestel, C. O. Rasmussen, and P. Z. Skands, Comput. Phys. Commun. **191**, 159 (2015).

[51] S. Frixione, P. Nason, and C. Oleari, J. High Energy Phys. 11 (2007) 070.

[52] R. Vogt, Phys. Rev. C **98**, 034907 (2018).

[53] R. Aaij *et al.* (LHCb Collaboration), J. High Energy Phys. 11 (2017) 030.

[54] S. Acharya *et al.* (ALICE Collaboration), J. High Energy Phys. 05 (2021) 220.

[55] R. Aaij *et al.* (LHCb Collaboration), J. High Energy Phys. 06 (2017) 147.

[56] L. Adamczyk *et al.* (STAR Collaboration), Phys. Rev. Lett. **113**, 142301 (2014); **121**, 229901(E) (2018).

[57] E. A. Remler, Ann. Phys. (N.Y.) **136**, 293 (1981).

[58] M. Gyulassy, K. Frankel, and E. a. Remler, Nucl. Phys. **A402**, 596 (1983).

[59] T. Song, J. Aichelin, and E. Bratkovskaya, Phys. Rev. C **107**, 054906 (2023).

[60] R. J. Fries, V. Greco, and P. Sorensen, Annu. Rev. Nucl. Part. Sci. **58**, 177 (2008).

[61] R. J. Fries, B. Muller, C. Nonaka, and S. A. Bass, Phys. Rev. C **68**, 044902 (2003).

[62] R. L. Workman and Others (Particle Data Group), Prog. Theor. Exp. Phys. **2022**, 083C01 (2022).

[63] S. Shlomo and M. Prakash, Nucl. Phys. **A357**, 157 (1981).

[64] S. Acharya *et al.* (ALICE Collaboration), J. High Energy Phys. 03 (2022) 190.

[65] S. Acharya *et al.* (ALICE Collaboration), J. High Energy Phys. 10 (2019) 084.

[66] M. Aaboud *et al.* (ATLAS Collaboration), Eur. Phys. J. C **78**, 171 (2018).

[67] A. M. Sirunyan *et al.* (CMS Collaboration), Phys. Lett. B **790**, 509 (2019).

[68] A. Adare *et al.* (PHENIX Collaboration), Phys. Rev. D **85**, 092004 (2012).

[69] J. Adam *et al.* (STAR Collaboration), Phys. Lett. B **786**, 87 (2018).

[70] A. M. Sirunyan *et al.* (CMS Collaboration), Phys. Lett. B **790**, 270 (2019).

[71] A. Tumasyan *et al.* (CMS Collaboration), Phys. Rev. Lett. **128**, 252301 (2022).

[72] D. Ebert, R. N. Faustov, and V. O. Galkin, Phys. Rev. D **68**, 094020 (2003).

[73] E. Hernandez, J. Nieves, and J. M. Verde-Velasco, Phys. Rev. D **74**, 074008 (2006).

[74] C.-F. Qiao and R.-L. Zhu, Phys. Rev. D **87**, 014009 (2013).